



Article

# Electrochemistry Studies of Hydrothermally Grown ZnO on 3D-Printed Graphene

Dimitra Vernardou <sup>1,\*</sup> and George Kenanakis <sup>2</sup>

<sup>1</sup> Center of Materials Technology and Photonics, School of Engineering, Hellenic Mediterranean University, 710 04 Heraklion, Crete, Greece

<sup>2</sup> Institute of Electronic Structure and Laser, Foundation for Research and Technology-Hellas, N. Plastira 100, Vasilika Vouton, GR-700 13 Heraklion, Crete, Greece

\* Correspondence: dvernardou@staff.hmu.gr; Tel.: +30-281-037-9753

Received: 9 July 2019; Accepted: 20 July 2019; Published: 23 July 2019



**Abstract:** A three-dimensional (3D) printer was utilised for the three-dimensional production of graphene-based pyramids and an efficient hydrothermal procedure for ZnO growth. In particular, the 3D-printed graphene pyramids were forwarded in Pyrex glass bottles with autoclavable screw caps filled with 50 mL of an aqueous solution of zinc nitrate hexahydrate and hexamethylenetetramine for 1 h at 95 °C; sufficient enough time to deposit well-dispersed nanoparticles. X-ray diffraction patterns were in accordance with a Raman analysis and presented the characteristic peaks of graphite along with those of wurtzite ZnO. Different positions on the sample were tested, confirming the uniform dispersion of ZnO on graphene pyramids. From the electrochemical studies, it was found that the charging and discharging processes are affected by the presence of ZnO, indicating one well-defined plateau for each process compared to the previously reported bare graphene pyramids. In total, the material shows a value of 325 mAh g<sup>-1</sup>, a capacitance retention factor of 92% after 5000 scans, and a coulombic efficiency of 100% for the first scan that drops to 85% for the 5000th scan. This excellent performance is the result of the effect of ZnO and graphene that combines two Li<sup>+</sup> accommodation sites, and the contribution of graphene pyramids, which provides more available sites to favor lithium storage capacity. Hence, this anode may be a promising electrode material for lithium-ion batteries.

**Keywords:** 3D-printed graphene; zinc oxide; hydrothermal growth; electrochemical studies

## 1. Introduction

Metal oxides have been widely investigated as electrodes for Li-ion batteries due to their high theoretical capacities, low cost and natural abundance [1,2]. In particular, ZnO has received increased attention as a large band gap semiconductor with distinctive photocatalytic, sensing and electrochemical properties [3–5]. As an anode material, it has a particularly high theoretical capacity of 978 mAh g<sup>-1</sup> (i.e., higher than that of graphite, which is 370 mA h g<sup>-1</sup>) [6], chemical stability and a lack of safety issues associated with its use. Nevertheless, achieving a high rate capability and good stability has been very challenging because of its low electronic conductivity and undesirable large volume change during its charging and discharging processes [7–10]. To tackle this drawback, one proposed strategy is to decrease the particle size of the metal oxide (i.e., to the nanoscale level). This will provide a larger area of active material, accommodating effectively the strain of Li intercalation/deintercalation in nanomaterials [11–13]. However, low conductivity and inferior cyclability remain critical issues limiting its application [14,15].

The exceptional conductivity, abundant adsorption sites and short diffusion paths associated with graphene are expected to further enhance the transport processes within the oxide nanomaterials [16]. A major advantage of graphene over other carbon materials is the excellent distribution of metal oxides

on its surface [17]. The advantages of ZnO/graphene composites were evaluated in many studies [18] estimating a reversible capacity of  $515 \text{ mAh g}^{-1}$  after 100 cycles at  $200 \text{ mA g}^{-1}$  [19], a high initial discharge capacity of  $1583 \text{ mAh g}^{-1}$  at  $200 \text{ mA g}^{-1}$  [11] and a reversible capacity of  $653.7 \text{ mAh g}^{-1}$  after 100 cycles [20].

In this work, ZnO is deposited on three-dimensional (3D)-printed graphene [21] using the environmentally friendly hydrothermal process [22] at  $95 \text{ }^\circ\text{C}$  for 1 h. The hydrothermal procedure and the printing technique are both considered to be low-cost and easily compatible with the production of electrodes with new shapes and compositions. Considering these aspects, the proposed material may make an important contribution to the fabrication of battery material technology.

## 2. Materials and Methods

Commercially available PLA (polylactic acid)-graphene filaments (purchased from BlackMagic3D, Ronkonkoma, NY, USA) with a volume resistivity of  $0.6 \text{ ohm-cm}$ , compatible with typical FDM (Fused Deposition Modeling) 3D printers, were used. As reported elsewhere [21], the development of graphene pyramids was carried out using a  $0.4 \text{ mm}$  nozzle at  $240 \text{ }^\circ\text{C}$ , while the surface where the object was printed was adjusted at  $50 \text{ }^\circ\text{C}$ . The 3D printing parameters (nozzle speed, extrusion velocity, layer thickness, printing path, etc.) were optimized in order to obtain uniformly printed samples with a filling ratio of 100%.

The 3D-printed PLA-graphene pyramids (as presented in [21]) were forwarded in Pyrex glass bottles with autoclavable screw caps filled with  $50 \text{ mL}$  of a  $0.01 \text{ M}$ , aqueous solution of  $\text{Zn}(\text{NO}_3)_2 \cdot 6\text{H}_2\text{O}$  and HMTA at  $95 \text{ }^\circ\text{C}$ . The HMTA acts as a reducing agent in the hydrothermal synthesis of ZnO [23]. In particular, it decomposes upon heating to form formaldehyde and ammonia, which then react with  $\text{H}_2\text{O}$  to produce  $\text{OH}^-$  and promote the precipitation reaction. Since the oxidation state of Zn in ZnO and  $\text{Zn}(\text{NO}_3)_2 \cdot 6\text{H}_2\text{O}$  is 2, the role of the reducing agent is in the nucleation and growth rate processes of ZnO materials instead of the reduction of  $\text{Zn}^{2+}$  ions [24]. After 1 h of deposition time, one could notice a white ZnO layer on the 3D-printed pyramids [22,23,25]. The composites were then washed with MilliQ  $\text{H}_2\text{O}$ , dried in air at  $95 \text{ }^\circ\text{C}$ , and characterized using the techniques described below. The growth temperature was carefully controlled with thermometers inside the oven and the Pyrex glass bottles during the whole growth period.

The surface morphology of the samples was determined using a field emission scanning electron microscope (FE-SEM, JEOL JSM-7000F, Tokyo, Japan) with a magnification of  $100\times$ . The crystal structure of all ZnO/3D-printed graphene samples was studied by X-ray diffraction (XRD, Rigaku (RINT 2000 diffractometer, Tokyo, Japan) with  $\text{Cu K}\alpha$  ( $\lambda = 1.5406 \text{ \AA}$ ). Raman measurements were carried out using a Horiba LabRAM HR (Kyoto, Japan) via a  $532 \text{ nm}$  solid state laser with an output power of  $100 \text{ mW}$  [21].

Electrochemical analysis of the materials was performed in an electrochemical cell [26] using Pt, Ag/AgCl and the ZnO/3D-printed graphene as the counter, reference and working electrode, respectively, in  $1 \text{ M LiCl}$  for a scan rate of  $10 \text{ mV s}^{-1}$  at potential ranging from  $-1.0 \text{ V}$  to  $+0.5 \text{ V}$ . Galvanostatic measurements were obtained in the range  $-0.5 \text{ V}$  to  $+0.5 \text{ V}$  under a specific current of  $40 \text{ mA g}^{-1}$ .

## 3. Results

### 3.1. Surface Morphology

Figure 1 depicts a typical SEM photograph of a ZnO/3D-printed graphene pyramid. The 3D structure of the printed samples can be clearly seen in Figure 1 to approach a truncated pyramid instead of an ideal square pyramid. Moreover, one can see from Figure 1 the layer-by-layer fabrication of the 3D-printed samples, with an  $\sim 100 \text{ }\mu\text{m}$  spatial resolution in the z-axis, which is a typical resolution for most FDM 3D printers.

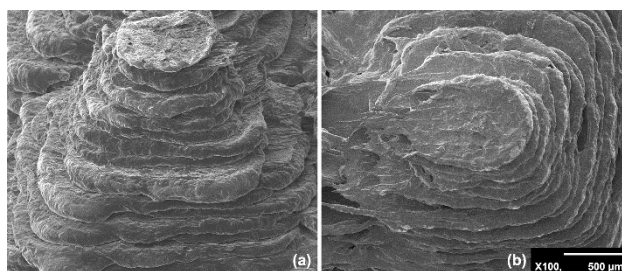


**Figure 1.** Typical SEM photographs of the ZnO/three-dimensional (3D)-printed graphene pyramids: (a) side view; (b) top view.

### 3.2. Structure

A typical XRD pattern of ZnO/3D-printed graphene samples is presented in Figure 2, verifying their crystalline properties. It depicts the characteristic peaks of the PLA profile [27], along with the graphite (JCPDS card, No.75-1621 [28,29]), indicating the existence of multilayered graphene in a PLA matrix. Finally, the XRD pattern of ZnO is identically matched with the characteristic peaks of ZnO's hexagonal P6(3)mc structure, in agreement with JCPDS card file No. 36-1451 and the literature [30].

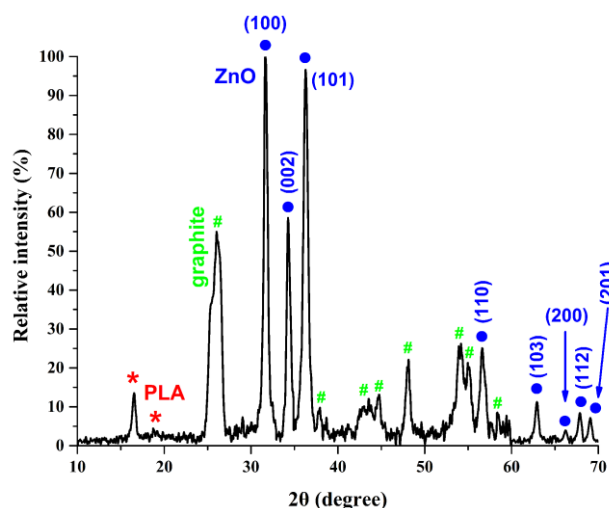


**Figure 2.** A typical XRD pattern of ZnO/3D-printed graphene samples. The XRD peaks of the graphite, PLA and ZnO are indicated with green hashes, red asterisks and blue dots, respectively.

A typical Raman spectrum of ZnO/3D-printed graphene samples is presented in Figure 3. The key features of the Raman spectrum at around  $1584$  and  $1356$   $\text{cm}^{-1}$  are the characteristic ones for carbon materials, the so-called G and D peaks. According to the literature associated with Raman analysis of graphene [31,32], the peak at  $1584$   $\text{cm}^{-1}$  ( $E_{2g}$  mode (G band) of graphite) is related to the vibration of  $sp^2$ -bonded carbon atoms. Additionally, the peak at  $1356$   $\text{cm}^{-1}$  is associated with the vibration of carbon atoms (D band). Accordingly, the phonon frequencies of the Raman spectra attributed to ZnO are:  $332$   $\text{cm}^{-1}$  (multiple-phonon scattering processes),  $379$   $\text{cm}^{-1}$  ( $A_1(\text{TO})$ ),  $438$   $\text{cm}^{-1}$  ( $E_2(\text{high})$ ),  $483$   $\text{cm}^{-1}$  ( $2\text{LA}$ ),  $574$   $\text{cm}^{-1}$  ( $A_1(\text{LO})$ ), and  $663$   $\text{cm}^{-1}$  ( $\text{TA}+A_1(\text{LO})$ ); which are in agreement with the literature [30,33–35], with the  $E_2(\text{high})$  mode at  $438$   $\text{cm}^{-1}$  exhibiting the strongest intensity. The rest peaks shown in the Raman spectrum of Figure 3 can be matched to the PLA of the materials. The Raman peak at  $1046$   $\text{cm}^{-1}$  can be assigned to the C–CH<sub>3</sub> stretching mode, whereas the one at  $871$   $\text{cm}^{-1}$  to the C–COO stretching of the polymer unit [36,37]. The samples were studied in different positions indicating similar spectra (as indicated in the inset of Figure 3), revealing the characteristic Raman peaks for graphene (G and D bands), along with the Raman fingerprints of PLA and ZnO, confirming the uniform dispersion of ZnO on 3D-printed graphene pyramids.

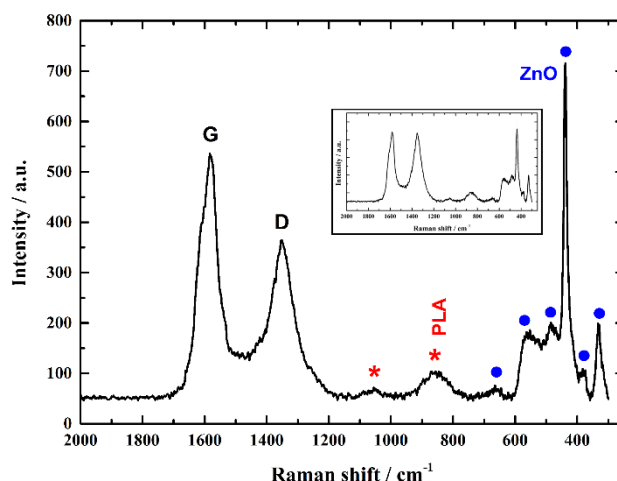


**Figure 3.** A typical Raman spectrum of ZnO/3D-printed graphene samples (PLA matrix and ZnO labeled with red asterisks and blue dots, respectively). In the inset of Figure 3, one can see a Raman spectrum at a different position of the same 3D-printed sample, indicating the uniform dispersion of ZnO on 3D-printed graphene pyramids.

### 3.3. Electrochemical Studies

Figure 4 indicates the cyclic voltammograms for 5000 scans sweeping the potential from  $-1.0$  V to  $+0.5$  V versus Ag/AgCl at  $10 \text{ mV s}^{-1}$ . The voltammogram for the first scan shows two cathodic humps at  $-0.60$  V/ $-0.19$  V and two respective anodic humps at  $-0.54$  V/ $+0.05$  V. Additionally, it may be seen that the anodic humps shift to higher potentials, whereas the cathodic humps to lower values after 2500 scans. Nevertheless, the curves are stable and overlap in subsequent scans, indicating that the material presents high electrochemical reversibility and stability after a prolonged period. The high resistivity of the cyclic voltammograms may be due to the low conductivity of the electrolyte solution or the graphene pyramids. Work on the electrochemical study of the material is currently in progress using a higher concentration of electrolyte solution and developing graphene pyramids on a conductive substrate.

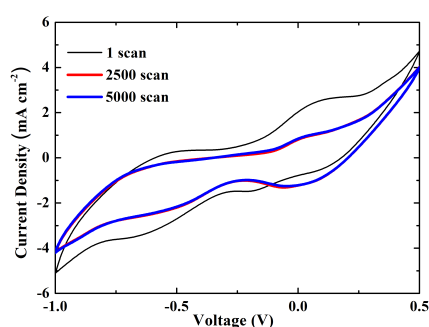


**Figure 4.** Cyclic voltammograms of ZnO/3D-printed graphene for  $10 \text{ mV s}^{-1}$  and a number of scans up to 5000.

The chronopotentiometric (CP) curves of the ZnO/3D-printed graphene for the first and the 5000th scan at  $40 \text{ mA g}^{-1}$  and a potential range of  $-0.50$  V to  $+0.50$  V are shown in Figure 5a. It may be observed that the charging and discharging processes are affected by the ZnO's presence, indicating one well-defined plateau for each process as compared with the bare graphene [21]. Additionally, the material shows a specific discharge capacity of  $325 \text{ mAh g}^{-1}$  and a capacitance retention factor of 92% after 5000 scans (Figure 5b). This excellent performance is due to the effect of ZnO and graphene that combines two  $\text{Li}^+$  accommodation sites [18]. In particular, the well-dispersed ZnO on the 3D-printed graphene network offers an additional redox site (apart from graphene; C element). Furthermore, the contribution of graphene pyramids provides high surface areas and more available sites to facilitate

the Li-storage capacity. The reduction of ZnO into Zn and the formation of a lithium–zinc alloy are proposed regarding the Li-redox reactions in the active sites of ZnO [38,39]. Accordingly, the electroactive sites in graphene pyramids for Li storage can be expressed according to the equation  $x\text{Li}^+ + \text{C}_6 + xe^- \leftrightarrow \text{Li}_x\text{C}_6$  [21]. In Table 1 below, the specific discharge capacity value and scan number of other anode materials are shown and compared with the one reported in this work. It is indicated that the anode material that was prepared by the combination of a 3D-printing technique and a hydrothermal procedure has not been reported before utilising either an organic or an inorganic electrolyte. The estimated capacity value after 5000 scans is promising for further exploitation in Li-ion batteries if one considers the low cost and the high safety of the materials technology along with the aqueous-based electrolytes, respectively.

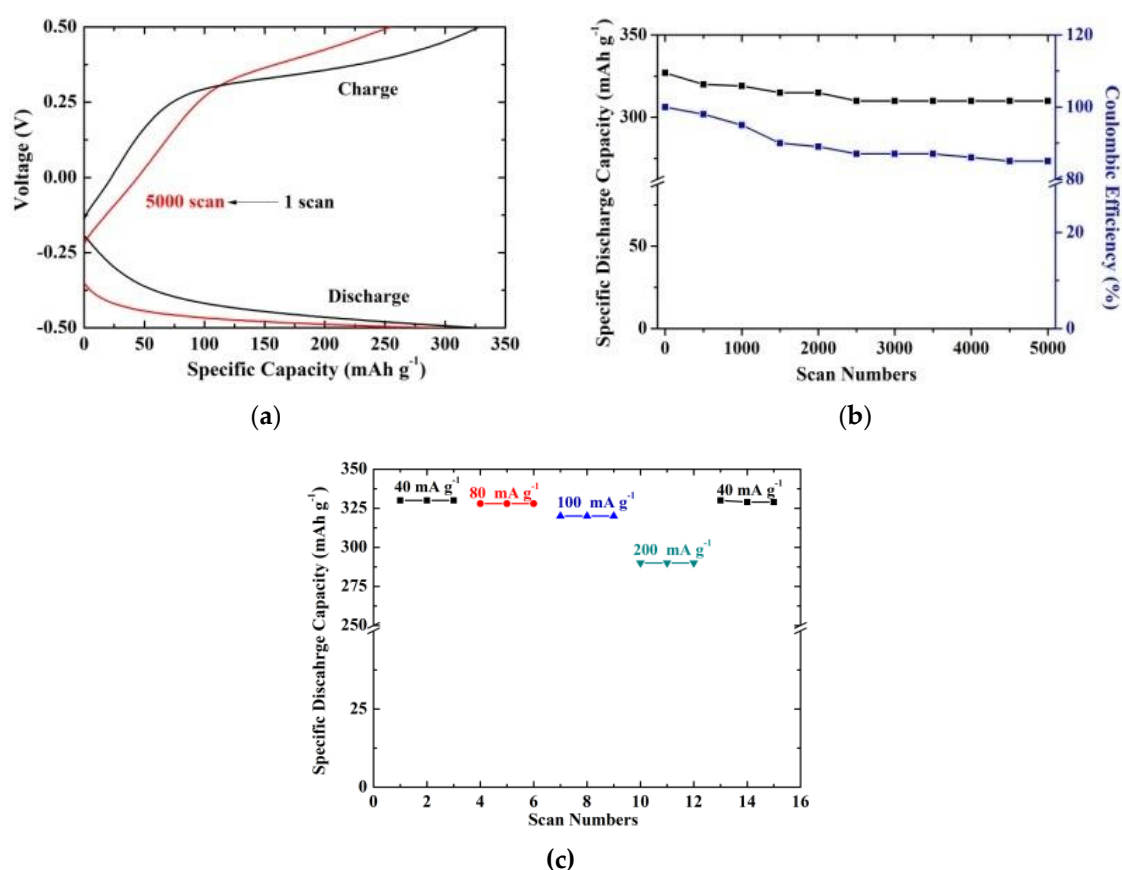


**Figure 5.** (a) The chronopotentiometric (CP) curves of ZnO/3D-printed graphene for  $-0.5$  V to  $+0.5$  V at  $40 \text{ mA g}^{-1}$  (the charge and discharge curves are indicated along with the 1st and the 5000th scan in black and red color, respectively); (b) Specific discharge capacity and coulombic efficiency of the anode material as a function of the scan numbers; (c) Rate capability of the composite at  $40$ ,  $80$ ,  $100$ ,  $200 \text{ mA g}^{-1}$  and then back to  $40 \text{ mA g}^{-1}$ .

**Table 1.** Coulombic efficiency and specific discharge capacity of anodes taken from the literature.

Anodes	Specific Discharge Capacity	Scan Number	References
ZnO-CoO-C	$438 \text{ mAh g}^{-1}$	50 (0.0–2.5 V)	[40]
ZnO/graphene	$250 \text{ mAh g}^{-1}$	100 (0.005–3.0 V)	[41]
ZnO-Loaded/Porous carbon composite	$512.7 \text{ mAh g}^{-1}$	10 (0.1–3.0 V)	[20]
ZnO nanorod	$358 \text{ mAh g}^{-1}$	30 (0.3–3.0 V)	[42]
3D-printed graphene	$265 \text{ mAh g}^{-1}$	1000 (−1.0–0.5 V)	[21]
ZnO/3D-printed graphene pyramids	$306 \text{ mAh g}^{-1}$	5000 (−1.0–0.5 V)	This work

The anode material exhibited a coulombic efficiency of 100% that dropped to 85% after 5000 scans as shown in Figure 5b. The coulombic efficiency observed in this material is much higher than that of

ZnO@GN anodes (82.1%) [18], SiO<sub>2</sub>@C hollow spheres (≈45%) [43] and carbon/ZnO nanorod array anodes (44%) [44], showing an excellent reversible capacity. Rate capability was also evaluated at specific currents of 40 mA g<sup>-1</sup>, 80 mA g<sup>-1</sup>, 100 mA g<sup>-1</sup>, and 200 mA g<sup>-1</sup> as presented in Figure 5c. The anode maintains a high value of 290 mAh g<sup>-1</sup> under a specific current of 200 mA g<sup>-1</sup>. Furthermore, it delivered a value of 322 mAh g<sup>-1</sup> when the specific current returned to 40 mA g<sup>-1</sup>, suggesting high reversibility of the electrode.

#### 4. Conclusions

Hydrothermally grown ZnO on 3D-printed graphene was accomplished at 95 °C for 1 h. The materials were crystalline and the ZnO was uniformly dispersed on graphene pyramids. The presence of both ZnO and 3D-printed graphene pyramids affected the electrochemical behavior of the anode, indicating a specific discharge capacity of 325 mAh g<sup>-1</sup> and a capacitance retention factor of 92% after 5000 scans. This excellent performance is due to the combination of two Li<sup>+</sup> accommodation sites from ZnO and graphene along with the contribution of graphene pyramids facilitating more available sites. Considering these outcomes, the proposed anode material may significantly contribute to the fabrication of battery materials technology.

**Author Contributions:** Growth of ZnO/3D-printed graphene, G.K.; basic characterisation of composites, G.K.; electrochemical analysis, D.V.; writing—original draft preparation, D.V. and G.K.

**Funding:** This research was co-financed by the European Union and Greek national funds through the Operational Program Competitiveness, Entrepreneurship and Innovation, under the call RESEARCH – CREATE – INNOVATE (acronym: POLYSHIELD; project code: T1EDK-02784).

**Conflicts of Interest:** The authors declare no conflicts of interest.

#### References

1. Ji, L.; Lin, Z.; Alcoutalabi, M.; Zhang, X. Recent development in nanostructured anode materials for rechargeable lithium-ion batteries. *Energy Environ. Sci.* **2011**, *4*, 2682–2699. [[CrossRef](#)]
2. Wu, H.B.; Chen, J.S.; Hng, H.H.; Lou, X.W. Nanostructured metal oxide-based materials as advanced anodes for lithium-ion batteries. *Nanoscale* **2012**, *4*, 2526–2542. [[CrossRef](#)] [[PubMed](#)]
3. Zhu, L.; Zeng, W. Room-temperature gas sensing of ZnO-based gas sensor: A review. *Sens. Actuator A Phys.* **2017**, *267*, 242–261. [[CrossRef](#)]
4. Ong, C.B.; Ng, L.Y.; Mohammad, A.W. A review of ZnO nanoparticles as solar photocatalysts: Synthesis, mechanisms and applications. *Renew. Sustain. Energy Rev.* **2018**, *81*, 536–551. [[CrossRef](#)]
5. Xiao, L.; Li, E.; Yi, J.; Meng, W.; Wang, S.; Deng, B.; Liu, J. Enhancing the performance of nanostructured ZnO as an anode material for lithium-ion batteries by polydopamine-derived carbon coating and confined crystallization. *J. Alloy. Compd.* **2018**, *764*, 545–554. [[CrossRef](#)]
6. Su, Q.M.; Dong, Z.M.; Zhang, J. Visualizing the electrochemical reaction of ZnO nanoparticles with lithium by in situ TEM: Two reaction modes are revealed. *Nanotechnology* **2013**, *24*, 255705. [[CrossRef](#)]
7. Zhang, Y.; Wei, Y.; Li, H.; Zhao, Y.; Yin, F.; Wang, X. Simple fabrication of free-standing ZnO/graphene/carbon nanotube composite anode for lithium-ion batteries. *Mater. Lett.* **2016**, *184*, 235–238. [[CrossRef](#)]
8. Zhao, Y.; Li, H.; Zhang, Y.; Xie, H.; Yin, F. One-pot synthesis of radial ZnO nanoparticles deposited on graphene nanosheets as the anode materials for lithium-ion batteries. *Int. J. Electrochem. Sci.* **2016**, *11*, 3179–3189. [[CrossRef](#)]
9. Belliard, F.; Irvine, J.T.S. Electrochemical performance of ball-milled ZnO-SnO<sub>2</sub> systems as anodes in lithium-ion battery. *J. Power Sources* **2001**, *97*, 219–222. [[CrossRef](#)]
10. Li, H.; Wei, Y.; Zhang, Y.; Yin, F.; Zhang, C.; Wang, G.; Bakonov, Z. Synthesis and electrochemical investigation of highly dispersed ZnO nanoparticles as anode material for lithium-ion batteries. *Ionics* **2016**, *22*, 1387–1393. [[CrossRef](#)]
11. Zhang, J.; Tan, T.; Zhao, Y.; Liu, N. Preparation of ZnO nanorods/graphene composite anodes for high-performance lithium-ion batteries. *Nanomaterials* **2018**, *8*, 966. [[CrossRef](#)] [[PubMed](#)]

12. Ahmad, M.; Shi, Y.; Nisar, A.; Sun, H.; Shen, W.; Wei, M.; Zhu, J. Synthesis of hierarchical flower-like ZnO nanostructures and their functionalization by Au nanoparticles for improved photocatalytic and high performance Li-ion battery anodes. *J. Mater. Chem.* **2011**, *21*, 7723–7729. [[CrossRef](#)]
13. Zhang, L.; Zhang, J.; Liu, Y.; Zheng, P.; Yuan, X.; Guo, S. Al doped-ZnO nanoparticles implanted in reduced graphene oxide with improved electrochemical properties for lithium ion batteries. *Mater. Lett.* **2016**, *165*, 165–168. [[CrossRef](#)]
14. Park, K.; Xia, F.; Kim, S.; Song, T.; Paik, U.; Park, W. Facile synthesis of ultrathin ZnO nanotubes with well-organized hexagonal nanowalls and sealed layouts: Applications for lithium ion battery anodes. *J. Phys. Chem. C* **2013**, *117*, 1037–1043. [[CrossRef](#)]
15. Xiao, L.; Mei, D.; Cao, M.; Qu, D.; Deng, B. Effects of structural patterns and degree of crystallinity on the performance of nanostructured ZnO as anode material for lithium-ion batteries. *J. Alloy Compd.* **2015**, *627*, 455–462. [[CrossRef](#)]
16. Li, F.; Jiang, X.; Zhao, J.; Zhang, S. Graphene oxide: A promising nanomaterial for energy and environmental applications. *Nano Energy* **2015**, *16*, 488–515. [[CrossRef](#)]
17. Wu, Z.S.; Zhou, G.; Yin, L.C.; Ren, W.; Li, F.; Cheng, H.M. Graphene/metal oxide composite electrode materials for energy storage. *Nano Energy* **2012**, *1*, 107–131. [[CrossRef](#)]
18. Hsieh, C.T.; Lin, C.Y.; Chen, Y.F.; Lin, J.S. Synthesis of ZnO@Graphene composites as anode materials for lithium ion batteries. *Electrochim. Acta* **2013**, *111*, 359–365. [[CrossRef](#)]
19. Li, H.; Wei, Y.; Zhang, Y.; Zhang, C.; Wang, G.; Zhao, Y.; Yin, F.; Bakenov, Z. In situ sol-gel synthesis of ultrafine ZnO nanocrystals anchored on graphene as anode material for lithium-ion batteries. *Ceram. Int.* **2016**, *42*, 12371–12377. [[CrossRef](#)]
20. Shen, X.; Mu, D.; Chen, S.; Wu, B.; Wu, F. Enhanced electrochemical performance of ZnO-loaded/porous carbon composite as anode materials for lithium ion batteries. *ACS Appl. Mater. Interfaces* **2013**, *5*, 3118–3125. [[CrossRef](#)]
21. Vernardou, D.; Vasilopoulos, K.C.; Kenanakis, G. 3D printed graphene-based electrodes with high electrochemical performance. *Appl. Phys. A* **2017**, *123*, 623. [[CrossRef](#)]
22. Kenanakis, G.; Androulidaki, M.; Vernardou, D.; Katsarakis, N.; Koudoumas, E. Photoluminescence study of ZnO structures grown by aqueous chemical growth. *Thin Solid Films* **2011**, *520*, 1353–1357. [[CrossRef](#)]
23. Vernardou, D.; Kenanakis, G.; Vlachou, K.; Koudoumas, E.; Kiriakidis, G.; Vairis, A.; Katsarakis, N. Influence of solution concentration and temperature on the aqueous chemical growth of zinc oxide growth. *Phys. Status Sol.* **2008**, *5*, 3348–3352. [[CrossRef](#)]
24. Thongam, D.D.; Gupta, J.; Sahu, N.K.; Bahadur, D. Investigating the role of different reducing agents, molar ratios, and synthesis medium over the formation of ZnO nanostructures and their photo-catalytic activity. *J. Mater. Sci.* **2018**, *53*, 1110–1122. [[CrossRef](#)]
25. Kenanakis, G.; Vernardou, D.; Koudoumas, E.; Katsarakis, N. Growth of c-axis oriented ZnO nanowires from aqueous solution: The decisive role of seed layer for controlling the wires' diameter. *J. Cryst. Growth* **2009**, *311*, 4799–4804. [[CrossRef](#)]
26. Vernardou, D.; Apostolopoulou, M.; Louloudakis, D.; Katsarakis, N.; Koudoumas, E. Hydrothermally grown  $\beta$ -V<sub>2</sub>O<sub>5</sub> electrode at 95 °C. *J. Colloid. Interf. Sci.* **2014**, *424*, 1–6. [[CrossRef](#)]
27. Teixeira, E.M.; de Campos, A.; Marconcini, J.M.; Bondancia, T.J.; Wood, D.; Klamczynski, A.; Mattoso, L.H.C.; Glenn, G.M. Starch/fiber/poly(lactic acid) foam and compressed foam composites. *RSC Adv.* **2014**, *4*, 6616–6623. [[CrossRef](#)]
28. Zhang, R.; Liu, Y.; Yu, L.; Li, Z.; Sun, S. Preparation of high-quality biocompatible carbon dots by extraction, with new thoughts on the luminescence mechanism. *Nanotechnology* **2013**, *24*, 225601–225608. [[CrossRef](#)]
29. Howe, J.Y.; Rawn, C.J.; Jones, L.E.; Ow, H. Improved crystallographic data for graphite. *Powder Diffr.* **2003**, *18*, 150–154. [[CrossRef](#)]
30. Vernardou, D.; Kenanakis, G.; Couris, S.; Koudoumas, E.; Kymakis, E.; Katsarakis, N. pH effect on the morphology of ZnO nanostructures grown with aqueous chemical growth. *Thin Solid Films* **2007**, *515*, 8764–8767. [[CrossRef](#)]
31. Park, S.H.; Bak, S.M.; Kim, K.H.; Jegal, J.P.; Lee, S.I.; Lee, J.; Kim, K.B. Solid-state microwave irradiation synthesis of high quality graphene nanosheets under hydrogen containing atmosphere. *J. Mater. Chem.* **2011**, *21*, 680–686. [[CrossRef](#)]

32. Shen, J.; Li, T.; Long, Y.; Shi, M.; Li, N.; Ye, M. One-step solid state preparation of reduced graphene oxide. *Carbon* **2012**, *50*, 2134–2140. [[CrossRef](#)]
33. Zhaochun, Z.; Baibiao, H.; Yongqin, Y.; Deliang, C. Electrical properties and Raman spectra of undoped and Al-doped ZnO thin films by metalorganic vapor phase epitaxy. *Mater. Sci. Eng. B* **2001**, *86*, 109–112. [[CrossRef](#)]
34. Cusco, R.; Alarcon-Liado, E.; Ibanez, J.; Artus, L.; Jimenez, J.; Wang, B.; Callahan, M.J. Temperature dependence of Raman scattering in ZnO. *Phys. Rev. B* **2007**, *75*, 165202. [[CrossRef](#)]
35. Cerqueira, M.F.; Viseu, T.; Ayres de Campos, J.; Rolo, A.G.; de Lacerda-Aroso, T.; Oliveira, F.; Bogdanovic-Radovic, I.; Alves, E.; Vasilevskiy, M.I. Raman study of insulating and conductive ZnO:(Al, Mn) thin films. *Phys. Status Solidi* **2015**, *212*, 2345–2354. [[CrossRef](#)]
36. Vano-Herrera, K.; Misiun, A.; Vogt, C. Preparation and characterization of poly(lactic acid)/poly(methyl methacrylate) blend tablets for application in quantitative analysis by micro Raman spectroscopy. *J. Raman Spectrosc.* **2015**, *46*, 273–279. [[CrossRef](#)]
37. Garlotta, D. A literature review of poly(lactic acid). *J. Polym. Environ.* **2001**, *9*, 63–84. [[CrossRef](#)]
38. Huang, X.H.; Xia, X.H.; Yuan, Y.F.; Zhou, F. Porous ZnO nanosheets grown on copper substrates as anode for lithium ion batteries. *Electrochim. Acta* **2011**, *56*, 4960–4965. [[CrossRef](#)]
39. Huang, X.H.; Wu, J.B.; Lin, Y.; Guo, R.Q. ZnO microrod arrays grown on copper substrates as anode materials for lithium ion batteries. *Int. J. Electrochem. Sci.* **2012**, *7*, 6611–6621.
40. Wu, Z.; Qin, L.; Pan, Q. Fabrication and electrochemical behaviour of flower-like ZnO-CoO-C nanowall arrays as anodes for lithium-ion batteries. *J. Alloy Compd.* **2011**, *509*, 9207–9213. [[CrossRef](#)]
41. Moon, Y.W.; Choi, I.J.; Koh, Y.H.; Kim, H.E. Porous alumina ceramic scaffolds with biomimetic macro/microporous structure using three-dimensional (3-D) ceramic/camphene-based extrusion. *Ceram. Int.* **2015**, *41*, 12371–12377. [[CrossRef](#)]
42. Lee, J.H.; Hon, M.H.; Chung, Y.W. The effect of TiO<sub>2</sub> coating on the electrochemical performance of ZnO nanorod as the anode material for lithium-ion battery. *Appl. Phys. A Mater. Sci. Process.* **2011**, *102*, 545–550. [[CrossRef](#)]
43. Liu, X.; Chen, Y.; Liu, H.; Liu, Z.Q. SiO<sub>2</sub>@C hollow sphere anodes for lithium-ion batteries. *J. Mater. Sci. Technol.* **2017**, *33*, 239–245. [[CrossRef](#)]
44. Liu, J.; Li, Y.; Ding, J.J.; Hu, Y.; Ji, X.; Chi, Q.; Zhu, Z.; Huang, X. Carbon/ZnO nanorod array electrode with significantly improved lithium storage capability. *J. Phys. Chem. C* **2009**, *113*, 5336–5339. [[CrossRef](#)]



© 2019 by the authors. Licensee MDPI, Basel, Switzerland. This article is an open access article distributed under the terms and conditions of the Creative Commons Attribution (CC BY) license (<http://creativecommons.org/licenses/by/4.0/>).